Article

Cell Reports

Microbiota-Driven Tonic Interferon Signals in Lung Stromal Cells Protect from Influenza Virus Infection

Graphical Abstract

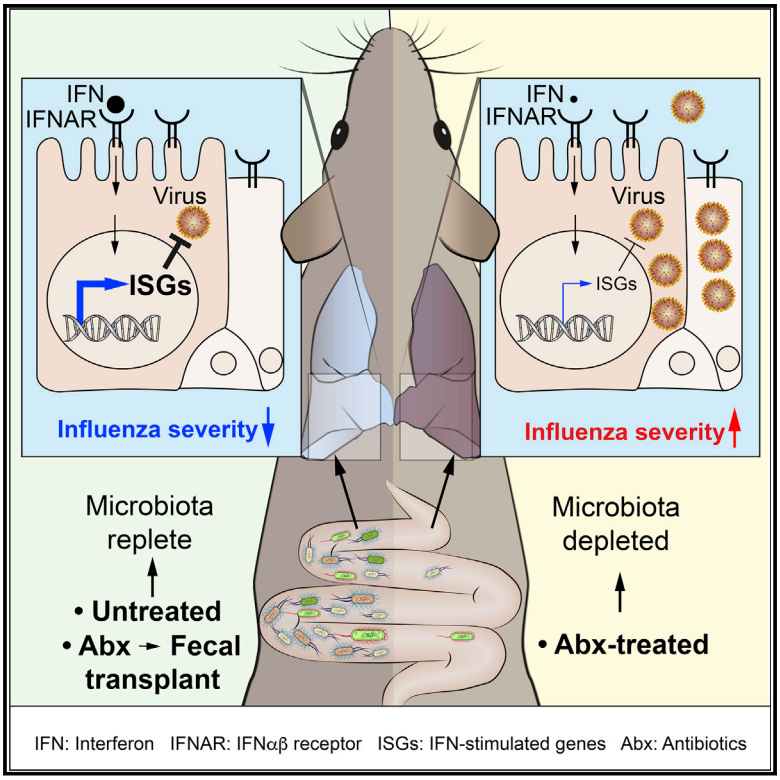

Authors

Konrad C. Bradley, Katja Finsterbusch, Daniel Schnepf, ..., Serge Y. Fuchs, Peter Staeheli, Andreas Wack

Correspondence

andreas.wack@crick.ac.uk

In Brief

Bradley, Finsterbusch, et al. identify lung stroma as the target of microbiota-driven signals that set the interferon signature in these cells. Antibiotic treatment reduces gut microbiota and the lung stromal interferon signature and facilitates early influenza virus replication in lung epithelia, effects that can be reversed by fecal transplantation.

Highlights

- Microbiota drive an interferon (IFN) signature in lung stroma cells
- Increased IFN signature impedes early influenza virus replication in lung epithelia
- IFN receptor levels fine-tune the IFN signature
- Antibiotics reduce the IFN signature and facilitate early virus replication

Bradley et al., 2019, Cell Reports *28*, 245–256
July 2, 2019
https://doi.org/10.1016/j.celrep.2019.05.105

CellPress

Cell Reports
Article

Microbiota-Driven Tonic Interferon Signals in Lung Stromal Cells Protect from Influenza Virus Infection

Konrad C. Bradley,[1,7] Katja Finsterbusch,[1,7] Daniel Schnepf,[2,3] Stefania Crotta,[1] Miriam Llorian,[4] Sophia Davidson,[1,8] Serge Y. Fuchs,[5] Peter Staeheli,[2,6] and Andreas Wack[1,9,*]

[1]Immunoregulation Laboratory, The Francis Crick Institute, 1 Midland Road, London NW1 1AT, UK
[2]Institute of Virology, University Medical Centre, Hermann-Herder-Straße 11, 79104 Freiburg, Germany
[3]Spemann Graduate School of Biology and Medicine, Albert Ludwigs University, Albertstraße 19A, 79104 Freiburg, Germany
[4]Bioinformatics STP, The Francis Crick Institute, 1 Midland Road, London NW1 1AT, UK
[5]Department of Biomedical Sciences, School of Veterinary Medicine, University of Pennsylvania, Philadelphia, PA 19104, USA
[6]Faculty of Medicine, University of Freiburg, Breisacher Straße 153, 79110 Freiburg, Germany
[7]These authors contributed equally
[8]Present address: Inflammation Division, The Walter and Eliza Hall Institute of Medical Research, Parkville, 3052, Australia
[9]Lead Contact
*Correspondence: andreas.wack@crick.ac.uk
https://doi.org/10.1016/j.celrep.2019.05.105

SUMMARY

Type I interferon (IFNα/β) pathways are fine-tuned to elicit antiviral protection while minimizing immunopathology; however, the initiating stimuli, target tissues, and underlying mechanisms are unclear. Using models of physiological and dysregulated IFNα/β receptor (IFNAR1) surface expression, we show here that IFNAR1-dependent signals set the steady-state IFN signature in both hematopoietic and stromal cells. Increased IFNAR1 levels promote a lung environment refractory to early influenza virus replication by elevating the baseline interferon signature. Commensal microbiota drive the IFN signature specifically in lung stroma, as shown by antibiotic treatment and fecal transplantation. Bone marrow chimera experiments identify lung stromal cells as crucially important for early antiviral immunity and stroma-immune cell interaction for late antiviral resistance. We propose that the microbiota-driven interferon signature in lung epithelia impedes early virus replication and that IFNAR1 surface levels fine-tune this signature. Our findings highlight the interplay between bacterial and viral exposure, with important implications for antibiotic use.

INTRODUCTION

Interferons (IFNs) were discovered by Isaacs and Lindenmann (1957) as host-produced antiviral substances. More than 60 years of research have established the critical importance to human health of type I IFN (IFNα/β), as it induces transcription of interferon-stimulated genes (ISGs) that encode proteins with various antiviral functions (Finter et al., 1991; García-Sastre and Biron, 2006; Isaacs and Lindenmann, 1957) in both infected and neighboring cells. Antiviral protection is established either by directly targeting the viral life cycle or by disrupting cellular metabolism and suppressing the translational machinery (Kristiansen et al., 2011; Pavlovic et al., 1992; Versteeg and García-Sastre, 2010). Induction of the antiviral state is necessary to restrict the damage caused by viral pathogens; however, emerging evidence shows that excessive production of IFN, driven either by pathogen (Bosinger and Utay, 2015; Chen et al., 1999; Li et al., 2018; Stifter and Feng, 2015; Teijaro et al., 2013; Utay and Douek, 2016; Wilson et al., 2013) or by host-encoded determinants (Davidson et al., 2014; Gougeon and Herbeuval, 2012; Jacquelin et al., 2009; Lee-Kirsch et al., 2007), can cause severe disease, as has been demonstrated for influenza, HIV infection, tuberculosis, lupus, and Aicardi-Goutiéres syndrome.

The dual nature of IFNα/β makes them a preferential target for regulation by both invading pathogens and host regulatory mechanisms. In fact, virus isolates that lack the ability to modulate the IFNα/β response (such as laboratory-rescued ΔNS1 influenza viruses) are severely attenuated *in vitro* and *in vivo* but can replicate in IFN-incompetent Vero cell lines (Egorov et al., 1998; García-Sastre et al., 1998), highlighting the importance of immunomodulation to viral fitness. Much research has focused on understanding the myriad mechanisms by which influenza A virus inhibits the IFNα/β response (Bergmann et al., 2000; García-Sastre, 2011; Rajsbaum et al., 2012; Versteeg and García-Sastre, 2010; Xia et al., 2015).

To avoid tissue damage and immune paralysis due to excessive IFNα/β signaling, host organisms have also evolved several levels of regulation of IFNα/β signaling (François-Newton et al., 2011; Gracias et al., 2013; Yoshimura et al., 2007). An important mechanism of IFNα/β regulation is the transient downregulation of IFNAR1 surface expression by targeted ubiquitination after signaling, which has been shown to be critical for protection against caerulin-induced pancreatitis and other inflammatory processes (Bhattacharya et al., 2014; Huangfu et al., 2012; Qian et al., 2011; Zheng et al., 2011). The importance of this host strategy in viral infection has yet to be established. Therefore, we aimed to understand how transient downregulation of

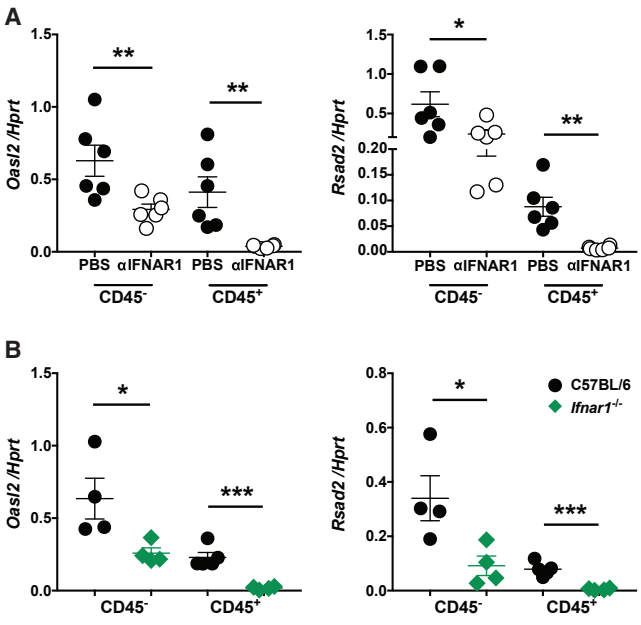

Figure 1. IFNAR1-Mediated Signals Determine Baseline ISG Signatures in Stromal and Hematopoietic Lung Cells

(A) ISG expression determined by qRT-PCR in magnetic-activated cell sorting (MACS)-separated $CD45^+$ and $CD45^-$ cells from the lungs of C57BL/6 mice (n = 6 samples from six animals) treated with αIFNAR1 antibody on days 0 and 2. Lungs were harvested on day 4.

(B) As in (A) from lungs of untreated C57BL/6 *Ifnar1*$^{+/+}$ and C57BL/6 *Ifnar1*$^{-/-}$ mice (n = 4 or 5 samples from four or five animals).

Expression levels of *Oasl2* and *Rsad2* are shown relative to transcription of the *Hprt* housekeeping gene. All bars represent mean ± SEM. Significance was determined using the Mann-Whitney U test: *p < 0.05, **p < 0.01, and ***p < 0.001.

IFNAR1 after stimulation can affect excessive IFNα/β signaling. We used mice homozygous for a point mutation at the IFNAR1 serine residue 526 (*Ifnar1*^{S526A}; hereafter *Ifnar1*^{SA} or SA^+), which are unable to ubiquitinate IFNAR1 following stimulation of the receptor complex, preventing the subsequent downregulation of IFNAR1 and thereby enhancing the IFN signal (Bhattacharya et al., 2014; Zheng et al., 2011). We find that regulation of IFNAR1 surface levels is the key to fine-tuning the degree of IFNα/β priming in the naive lung. As a consequence, *Ifnar1*^{SA} mice are more resistant to influenza virus infection, because of increased baseline ISG levels. Moreover, we show that in both wild-type (WT) and *Ifnar1*^{SA} mice, microbiota enhance the IFNAR1-driven ISG expression specifically in epithelial cells. Thus, lung epithelia are important receivers of tonic signals that determine the strength of subsequent, infection-induced IFNα/β signaling and promote resistance to viral infection.

RESULTS

IFNAR1-Dependent Signals Drive the ISG Signature in Lung Stromal and Hematopoietic Cells

Baseline activation of the IFN pathway in uninfected animals has been hypothesized to be due to tonic IFNβ signaling (Gough et al., 2012). To explore whether this applies to both hematopoietic and stromal cells, we measured ISG levels in CD45-positive and CD45-negative lung cells. First, we delivered two doses of αIFNAR1 antibody (MAR1) separated by 48 h, followed by harvesting lungs on day 2 post-second injection into C57BL/6 mice. Both cell populations showed a clear downregulation of classical ISGs such as *Rsad2* and *Oasl2* upon treatment, indicating that tonic levels of IFN signaling drive the ISG baseline in these cell compartments (Figure 1A). Accordingly, lower levels of ISG expression were found in both cell populations in lungs from IFNAR1-deficient (*Ifnar1*$^{-/-}$) mice in which IFNα/β signaling is constitutively absent (Figure 1B), indicating that steady-state ISG levels are driven by IFNAR1-dependent signals both in hematopoietic and stromal cells.

IFNAR1 Levels Regulate ISG Baseline Expression and IFN-Driven Immune Responses

The above results show that IFNAR1-mediated signals are required to maintain the lung baseline ISG signature, and tuning IFNAR1 levels is one way of controlling the magnitude of the IFN signal (Levin et al., 2011; Liu et al., 2009; Moraga et al., 2009). We therefore used *IFNAR1*^{SA} mice that express a variant of the IFNAR1 receptor chain that is not ubiquitinated and as a result cannot be degraded after ligand binding and signaling via the JAK/STAT pathway, leading to prolonged IFN signaling because of the inability to shut down the signal (Bhattacharya et al., 2014; Zheng et al., 2011). To confirm this lack of IFNAR1 downregulation, we first treated bone marrow-derived macrophages (BMDMs) with limiting dilutions of $IFN\alpha_4$. Upon IFN treatment, BMDMs from *Ifnar1*$^{+/+}$ C57BL/6 mice downregulated surface expression of IFNAR1 in a dose-dependent manner, whereas cells derived from *Ifnar1*^{SA} mice maintained nearly constant IFNAR1 expression for the lower $IFN\alpha_4$ concentrations (Figures 2A and S1A). Fluorescence-activated cell sorting (FACS) analysis of cells from naive *Ifnar1*^{SA} lungs showed elevated baseline IFNAR1 expression levels on both $CD45^+$ immune cells and $CD45^-$ epithelial and endothelial cells (Figures 2B, 2C, S1B, and S1C), indicating that continuous IFNAR1 degradation contributes to setting the physiological cell surface IFNAR1 levels in a dynamic equilibrium. Steady-state ISG expression was elevated in the lungs of *Ifnar1*^{SA} mice (Figure 2D), showing that IFNAR1 surface levels control the ISG signature. IFNAR1 blockade led to a rapid reduction of ISG levels, indicating that the ISG signature is in a dynamic equilibrium requiring constant IFN signals (Figure 2E). Importantly, we found increased ISG levels in both stromal and hematopoietic cells (Figure 2F), and surface expression of IFN-inducible Sca-1 and PDCA1 proteins was elevated on *Ifnar1*^{SA} lung immune cells compared with C57BL/6 (Figure S1D). Together, these data show that cell surface IFNAR1 levels regulate physiological levels of ISG expression in both stromal and hematopoietic cell compartments. This finding has important implications for lung immunity, as constitutive activation of the type I IFN pathway is emerging as a significant mechanism of immune homeostasis at mucosal sites of uninfected mice (Gough et al., 2012; Kawashima et al., 2013).

Changes in the baseline ISG expression in immune cells did not correspond to alterations in the immune cell composition

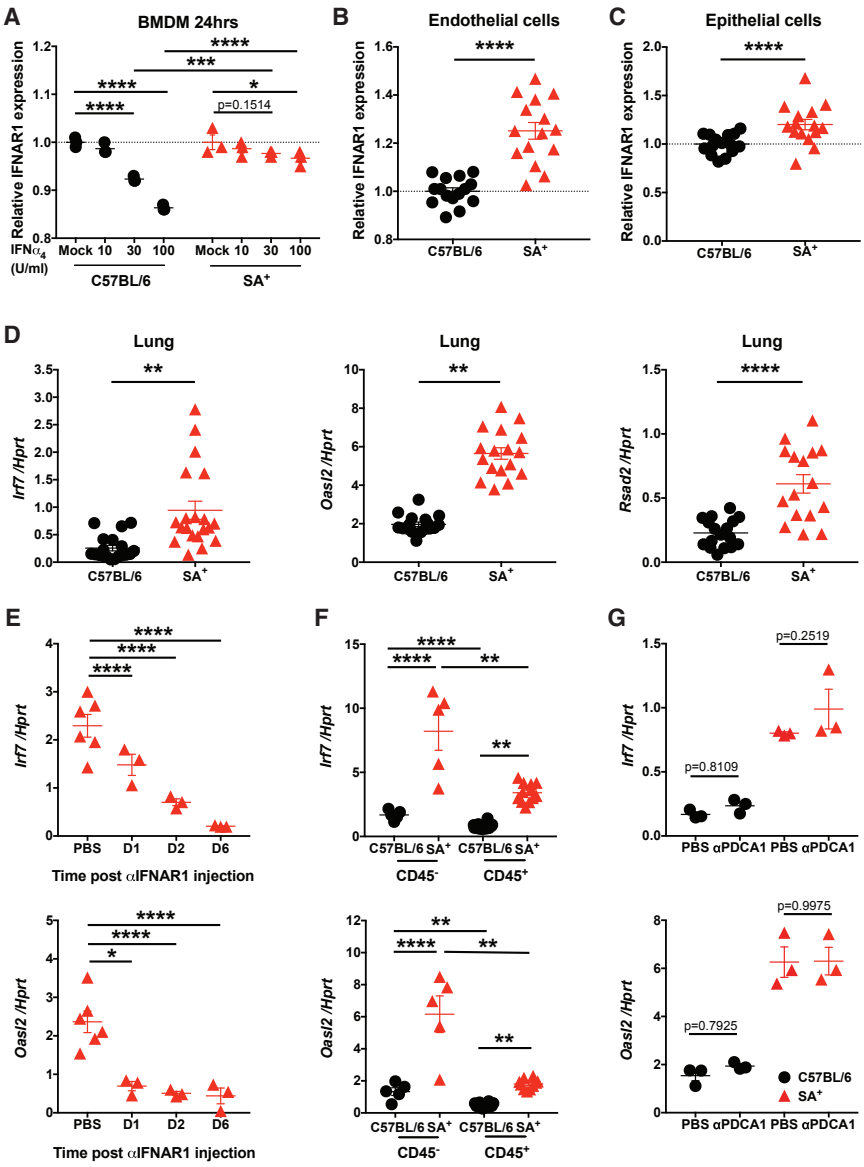

Figure 2. IFNAR1 Levels Tune Baseline ISG Expression in Lung Stroma and Immune Cells

(A) Surface IFNAR1 expression determined by flow cytometry of bone marrow-derived macrophages (BMDMs) stimulated with varying concentrations of IFNα_4 for 24 h. IFNAR1 expression was normalized to respective mock-treated BMDMs. n = 3 mice per group, 2 × 10^5 cells per animal.

(B and C) Relative IFNAR1 expression on epithelial cells ($CD45^-$, $EPCAM^+$) (B) or endothelial cells ($CD45^-$ $CD31^+$) (C) determined by flow cytometry and normalized to the respective C57BL/6 cell populations. Dashed line indicates mean of C57BL/6-derived cells. n = 15 mice per group.

(D) ISG expression determined by qRT-PCR in whole lungs of C57BL/6 or *Ifnar1*^{SA} mice (n = 17 per group).

(E) ISG expression determined by qRT-PCR decreases rapidly in the lungs of *Ifnar1*^{SA} mice (n = 3–6 per group) after treatment with αIFNAR1 antibody. Treatment delivered either once on day 0 (day 1 and day 2 harvests) or every 48 h (day 6 harvest).

(F) $CD45^+$ and $CD45^-$ MACS-separated cells from whole lungs of C57BL/6 or *Ifnar1*^{SA} mice (n = 5–12 per group) were analyzed for ISG expression by qRT-PCR.

(G) Depletion of pDCs does not reduce baseline ISG expression in *Ifnar1*^{SA} mice. Mice (n = 3 per group) treated with 400 μg αPDCA1 on day 0, day 2, and day 4. Whole lungs harvested on day 6 for gene expression analysis by qRT-PCR.

All gene expressions shown as relative to *Hprt* housekeeping gene. All bars represent mean ± SEM. Results are compiled from at least two experiments. Significance was determined using the Mann-Whitney U test (B, C, D, and G), 2-way ANOVA with Tukey's multiple comparisons test (A and F), or 1-way ANOVA (E): *p < 0.05, **p < 0.01, ***p < 0.001, and ****p < 0.0001.

of *Ifnar1*^{SA} mouse lungs (Figure S1E). This is in line with unaltered immune cell composition in the lungs of *Ifnar1*$^{-/-}$ mice (Figure S1F), indicating that a tonic type I IFN signal maintains the IFN signature in immune cells, but not their steady-state survival or recruitment. A notable exception is plasmacytoid dendritic cells (pDCs), whose numbers are reduced in the absence of IFN signaling (Figure S1F), in line with published observations (Kadowaki et al., 2000). pDCs are both maintained by and an important source of type I IFNs. To determine whether the ISG expression observed in WT and *Ifnar1*^{SA} mice was due to pDC-derived IFN, we used depleting antibodies against PDCA1, a primary marker for pDCs. Depletion of pDCs did not alter ISG expression in lungs (Figure 2G), indicating that other cells are responsible for establishing the baseline ISG expression in WT and *Ifnar1*^{SA} mice.

Ifnar1^{SA} Mice Are Less Susceptible to Influenza Virus Infection

Given the protective and pathological potential of type I IFNs, we wanted to test whether reduced IFNAR1 downregulation enhances immunopathology or facilitates immune-mediated protection during influenza virus infection. We found that *Ifnar1*^{SA} mice were more resistant to influenza virus infection than WT mice (Figure 3A). Virus gene expression (Ward et al., 2004) was significantly reduced at 8 h, and influenza virus replication was significantly reduced at 2 days post-infection in *Ifnar1*^{SA} mice (Figures 3B and 3C). To confirm this in a more clinically relevant infection model, we performed influenza virus infection of WT or *Ifnar1*^{SA} mice that carry a transgene encoding human MxA, the major restriction factor for influenza virus in humans (Deeg et al., 2017). When these mice were infected with a highly

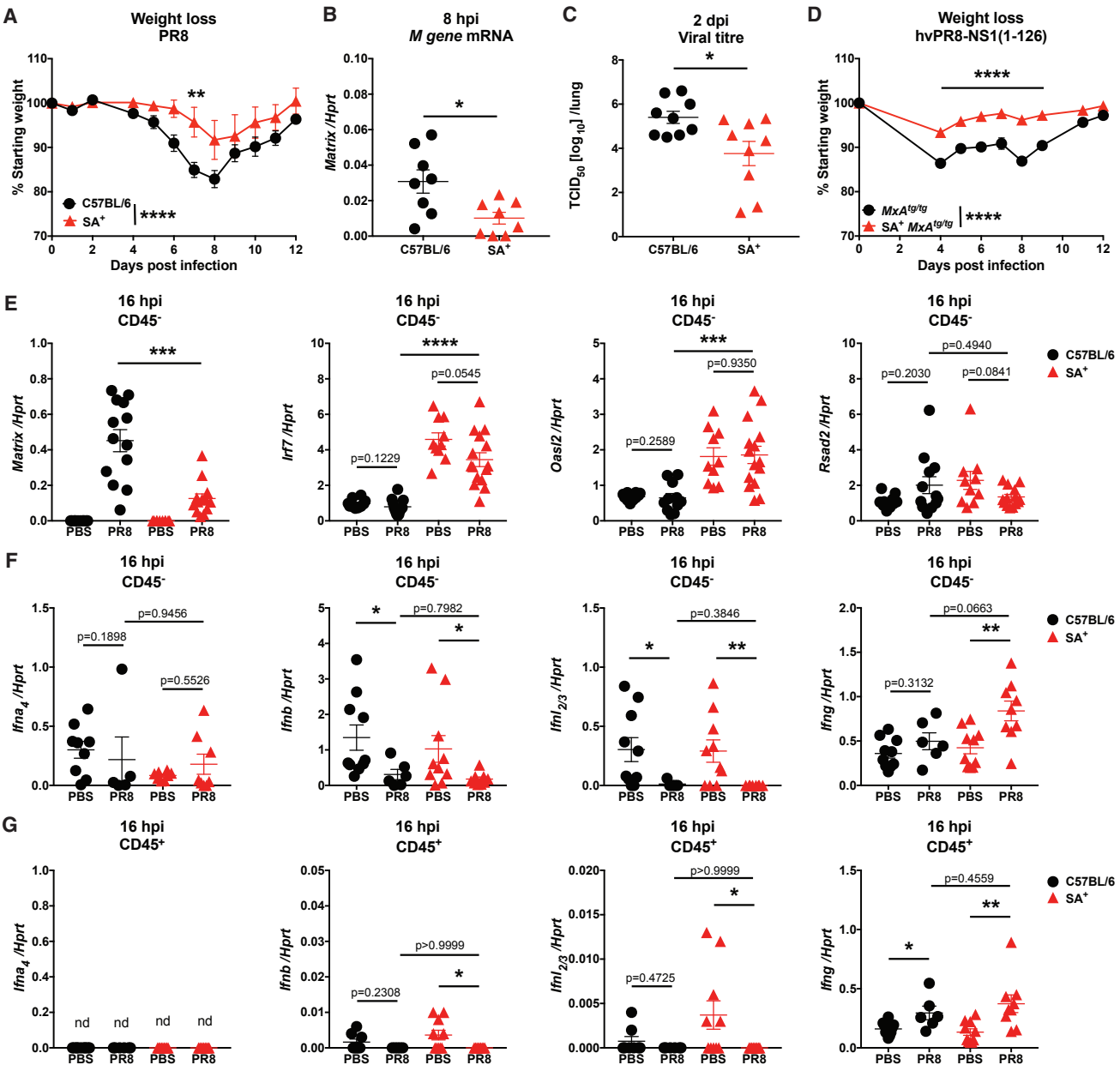

Figure 3. Increased Lung ISG Signature Protects from Influenza Virus Infection by Blunting Infection Early

(A) Weight loss of *Ifnar1*^{SA} and C57BL/6 mice (n = 5 per group) upon intranasal infection with 50 $TCID_{50}$ PR8 virus.

(B) Total *M gene* mRNA at 8 h post-infection with 1,000 $TCID_{50}$ PR8 delivered intranasally, as determined by qRT-PCR on cDNA created with oligo(dT) primers (n = 8 mice per group).

(C) Viral load determined using standard $TCID_{50}$ assay on Madin-Darby canine kidney (MDCK) cells. Mice (n = 9 per group) were infected with 8,000 $TCID_{50}$ X31 virus and lungs harvested on day 2.

(D) *MxA*$^{tg/tg}$ and *Ifnar1*^{SA}*MxA*$^{tg/tg}$ mice (n = 11 per group) were infected intranasally with 2,500 plaque-forming units (PFU) hvPR8-NS1(1-126) and monitored for weight loss.

(E–G) MACS-separated CD45^{-} (E and F) and CD45^{+} (G) cells from lungs of *Ifnar1*^{SA} and C57BL/6 mice (n = 5–15 per group) were used to determine viral load and ISG expression (E) or IFN expression (F and G) using qRT-PCR. Mice were intranasally infected with PBS or 2,000 $TCID_{50}$ PR8 virus for 16 h. cDNA was synthesized using oligo(dT) primers.

Results are compiled from at least two separate experiments. All bars represent mean ± SEM. Significance was determined using either two-way ANOVA with Sidak's multiple comparisons test (A and D) or the Mann-Whitney U test (B, C, and E–G): *p < 0.05, **p < 0.01, ***p < 0.001, and ****p < 0.0001. hpi, hours post-infection.

virulent variant of PR8 virus harboring a truncation in the IFN antagonist NS1 (Kochs et al., 2009), we found less weight loss in *Ifnar1*^{SA}*MxA*$^{tg/tg}$ mice than in controls (Figure 3D), similar to the above results (Figure 3A).

To test if the pre-existing ISG levels or increased responsiveness conferred antiviral protection in *Ifnar1*^{SA} mice, we measured the antiviral state in lung stromal cells. Reduced viral burden in *Ifnar1*^{SA} stromal cells corresponds to higher ISG levels in these cells compared with WT mice (Figure 3E) at 16 h post-infection, a time point at which we could not detect a further infection-mediated increase in ISG levels in WT or *Ifnar1*^{SA} mice. Correspondingly, neither stromal cells nor immune cells showed induction of IFN mRNAs this early in infection (Figures 3F and 3G). Similarly, no increase in ISG levels was found in stroma or immune cells at 8 h post-infection, when virus load was already reduced in *Ifnar1*^{SA} mice (Figures S2D and S2E versus Figure 3B). These results indicate that the pre-existing antiviral state, not rapid ISG upregulation, determines the observed early blunting of viral replication.

In line with this interpretation, we found reduced, not increased, IFN protein levels at 48 h post-infection (Figure S2A) in *Ifnar1*^{SA} mice. At this time point, immune cell recruitment into the lung is not different between WT and *Ifnar1*^{SA} mice (Figure S2B). Proinflammatory cytokines were also reduced at 5 days post-infection in *Ifnar1*^{SA}*MxA*$^{tg/tg}$ mice (Figure S2C). Together, these data demonstrate that the IFN-driven steady-state ISG signature in lung stroma is an important determinant of early anti-influenza control that subsequently leads to reduced immune responses, because of reduced viral load.

An alternative explanation for the reduced immune response was that *Ifnar1*^{SA} mice are intrinsically less reactive. We tested this and found *in vitro* higher reactivity of *Ifnar1*^{SA} airway epithelial cultures to IFNα and *in vivo* a higher immune cell recruitment into poly(I:C)-treated *Ifnar1*^{SA} lungs compared with WT controls, confirming previous findings (Bhattacharya et al., 2014; Figures S2F and S2G). The reduced immune response we find in influenza virus-infected *Ifnar1*^{SA} mice is therefore a direct consequence of reduced virus load as early as 8 h into the infection.

Elevated ISG Expression in CD45$^-$ Cells Is Critical for Early Protection against Influenza Virus Infection

To demonstrate the relative contributions of both CD45$^+$ and CD45$^-$ cells in the resistance of *Ifnar1*^{SA} mice to influenza virus, we created bone marrow (BM) chimeras between C57BL/6 and *Ifnar1*^{SA} mice. Chimeras were infected 6–8 weeks after BM reconstitution. As in previous experiments, all *Ifnar1*^{SA} chimeras exhibited considerably less weight loss than their C57BL/6 counterparts (Figure 4A). Additionally, C57BL/6 mice that received *Ifnar1*^{SA} BM displayed significantly greater weight loss than *Ifnar1*^{SA} recipients (Figure 4B). In particular, these mice showed more severe signs of disease during the first days of viral infection, suggesting that CD45$^-$ cells are critical to early blunting of virus-induced illness. Conversely, *Ifnar1*^{SA} mice that received WT BM lost more weight late during infection compared with controls receiving *Ifnar1*^{SA} BM (Figure 4C). To confirm that different cellular compartments contribute to protection early and late in infection, we performed 2-way ANOVA on the relative body weight values on day 3 and day 9 post-infection. We find that the source of variation on day 3 is the stroma genotype, while the source of variation on day 9 is interaction between stroma and BM genotypes (Figure 4D). These data demonstrate that IFNAR1-driven signals in CD45$^-$ cells are required to confer early protection, while IFNAR1-driven signals on hematopoietic cells contribute to protection in the later stage of infection.

Microbiota Drive the Steady-State ISG Signature in Lung Stroma but Not Immune Cells

To better understand the cause of elevated ISG levels in *Ifnar1*^{SA} mice, we first tested the hypothesis of a unique microflora in the *Ifnar1*^{SA} colony. When WT mice were co-housed for 1 month with *Ifnar1*^{SA} mice, whole-lung homogenates revealed no change in ISG expression in either WT or *Ifnar1*^{SA} mice or because of co-housing, and the increase in *Ifnar1*^{SA} over WT mice was maintained (Figure S3A). These results indicate that elevated ISG expression in the *Ifnar1*^{SA} mice is not due to their particular microflora.

Mice treated with oral antibiotics are more susceptible to viral infections, including influenza A virus (Abt et al., 2012; Goulding et al., 2011; Ichinohe et al., 2011; Oh et al., 2016; Steed et al., 2017), partly by regulating the activation threshold of the immune response. To determine whether ISG expression in the lung was directly affected by the microbiota, we treated mice with a cocktail of antibiotics *ad libitum* via their drinking water for 4 weeks and compared ISG expression in lungs of untreated and antibiotic-treated WT and *Ifnar1*^{SA} mice. No treatment-induced ISG difference was found when whole lungs were evaluated (Figure 5A); however, separation of CD45$^-$ and CD45$^+$ cells revealed a decline in ISG expression in the stromal compartment but not in cells of hematopoietic origin (Figures 5B and 5C).

Microbiota Drive Anti-influenza Virus Protection in Lung Stroma

To see if elevated ISG expression and the associated antiviral state might lead to stronger resistance, we first tested whether in *Ifnar1*^{SA} mice, reduction of ISGs by antibiotics relieves the viral replication block. To test this hypothesis, WT and *Ifnar1*^{SA} mice were treated with or without antibiotics for 4 weeks, followed by infection with influenza virus. As shown above (Figure 3A), untreated *Ifnar1*^{SA} mice were more resistant to influenza virus infection compared with their C57BL/6 counterparts. However, antibiotic-treated *Ifnar1*^{SA} mice were as susceptible as WT controls, indicating that microbiota-driven signals are responsible for the resistance phenotype found in *Ifnar1*^{SA} mice (Figure 5D). However, antibiotic treatment did not lead to significant changes in resistance of WT mice, which may be due to the lack of the critical influenza restriction factor, MX1, in most inbred mouse strains, including C57BL/6 mice. We therefore repeated experiments in *Mx1*-competent mice (Mordstein et al., 2008), a model that more closely reflects the human host situation in which a functional Mx gene (*MxA*) is present. We find that in *Mx1*$^{+/+}$ mice, antibiotics treatment significantly increased viral gene expression and viral replication early in infection (Figures 5E and 5F), indicating that the presence of the relevant influenza

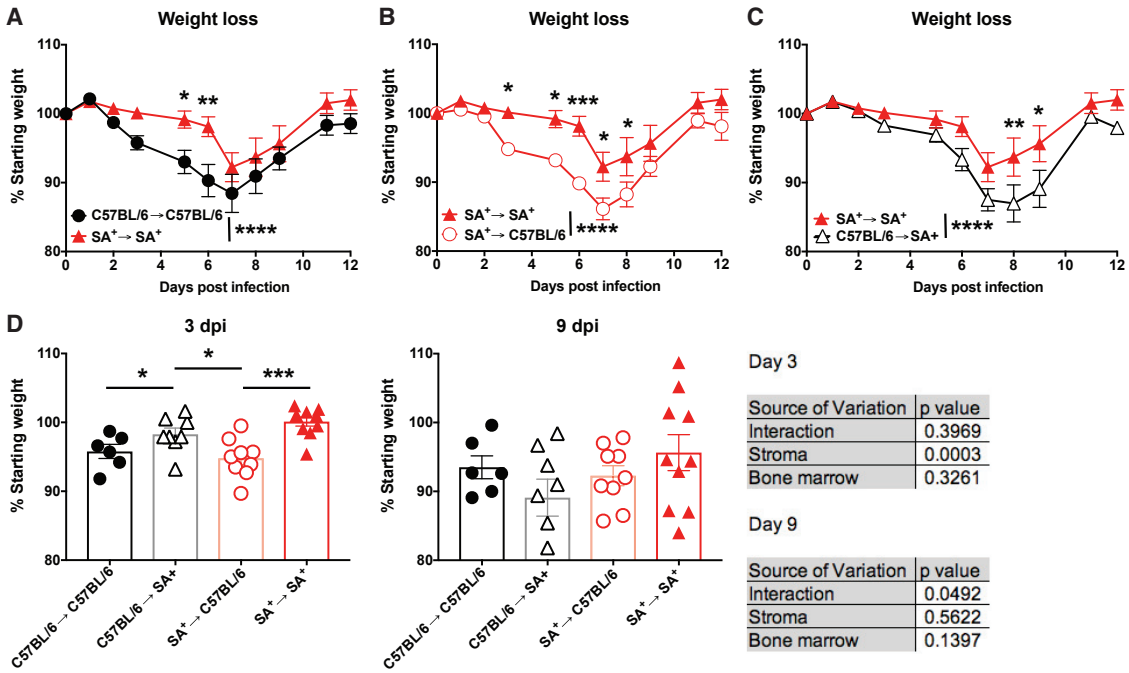

Figure 4. Stromal and Immune Cells Both Contribute to Resistance of *Ifnar1*^{SA} Mice to Influenza Infection

(A–C) Lethally irradiated WT or *Ifnar1*^{SA} mice (n = 6–10 per group) were reconstituted with 10^7 cells from either WT or *Ifnar1*^{SA} BMs. Mice were infected with 8,000 $TCID_{50}$ X31 and monitored for weight loss. Groups are represented by black closed circles (C57BL/6 donor into C57BL/6 recipient, A), red closed triangles (*Ifnar1*^{SA} donor into *Ifnar1*^{SA} recipient, A–C), red open circles (*Ifnar1*^{SA} donor into C57BL/6 recipient, B), and black open triangles (C57BL/6 donor into *Ifnar1*^{SA} recipient, C).

(D) Detailed representation and 2-way ANOVA of weight loss at day 3 and day 9 of the experiment described in (A)–(C).

Results shown are compiled from two separate weight-loss experiments; bars represent mean ± SEM. Statistical significance was determined using 2-way ANOVA with Tukey's multiple-comparisons test (A–C) or 2-way ANOVA using stroma and BM genotypes as factors, with Sidak's multiple-comparisons test (D): *p < 0.05, **p < 0.01, ***p < 0.001, and ****p < 0.0001. dpi, days post-infection.

restriction factor reveals the effect of the microbiota on early influenza virus control.

We expanded these findings and found that both in *Mx1*$^{+/+}$ *Ifnar1*^{wt} and *Mx1*$^{+/+}$*Ifnar1*^{SA} mice, antibiotic treatment significantly increased weight loss and mortality, while the *Mx1*$^{+/+}$ mice expressing *IFNAR1*^{SA} still tended to be better protected than their WT counterparts (Figure 6A). Consistent with loss of early virus control, we find elevated virus load at 16 h post-infection in antibiotic-treated mice (Figure 6B). Because antibiotic treatment reduces the antiviral state specifically in lung stromal cells (Figures 5B and 5C), our results indicate that the microbiota-driven IFN priming in the lungs acts on stromal cells to establish an antiviral state able to blunt influenza virus infection at the earliest stages.

To further confirm that gut microbiota are indeed responsible for the observed changes in baseline ISG expression, we treated antibiotic-exposed mice with fecal material of control mice through oral gavage (fecal transplantation [FT]). This treatment reversed the antibiotic-induced ISG reduction in lung stromal cells (Figure 6C). These effects were found both in *Ifnar1*^{wt} and *Ifnar1*^{SA} mice. In a more global analysis, we performed RNA sequencing on lung stroma from untreated, antibiotic-treated (Abx), and Abx/FT-treated mice (Figure 6D). Unbiased gene set enrichment analysis (GSEA) performed against the MsigDB database showed that the top pathway reduced in lung stroma from Abx mice is IFNα/β signaling, and several more immune- and IFN-related pathways were found among the ten top-scoring pathways (Figures 6D and 6E). In addition, all these pathways were enhanced by FT treatment. Table S1 lists the genes from the two (largely overlapping) top-scoring IFN-related pathways that we found differentially expressed in our treatment groups and that are shown in Figure 6E. Consistently, FT treatment reversed the antibiotic-induced susceptibility to influenza virus infection (Figure 6F). Taken together, these results demonstrate that the presence of microbiota increases the IFN-driven antiviral state in lung stroma and thereby increases protection from influenza virus infection.

DISCUSSION

Here, we identify tonic, microbiota-driven signals to lung stromal cells as a homeostatic mechanism that keeps epithelial cells in an IFN-primed state and thereby renders mice resistant to influenza virus infection through early blunting of the viral life cycle. We show that constant IFNα/β signaling is required, as antibody-mediated IFNAR1 blockade reduces the primed state within 24–48 h of treatment. Taking advantage of mice in which IFNAR1 downregulation is impaired by targeted mutation of a

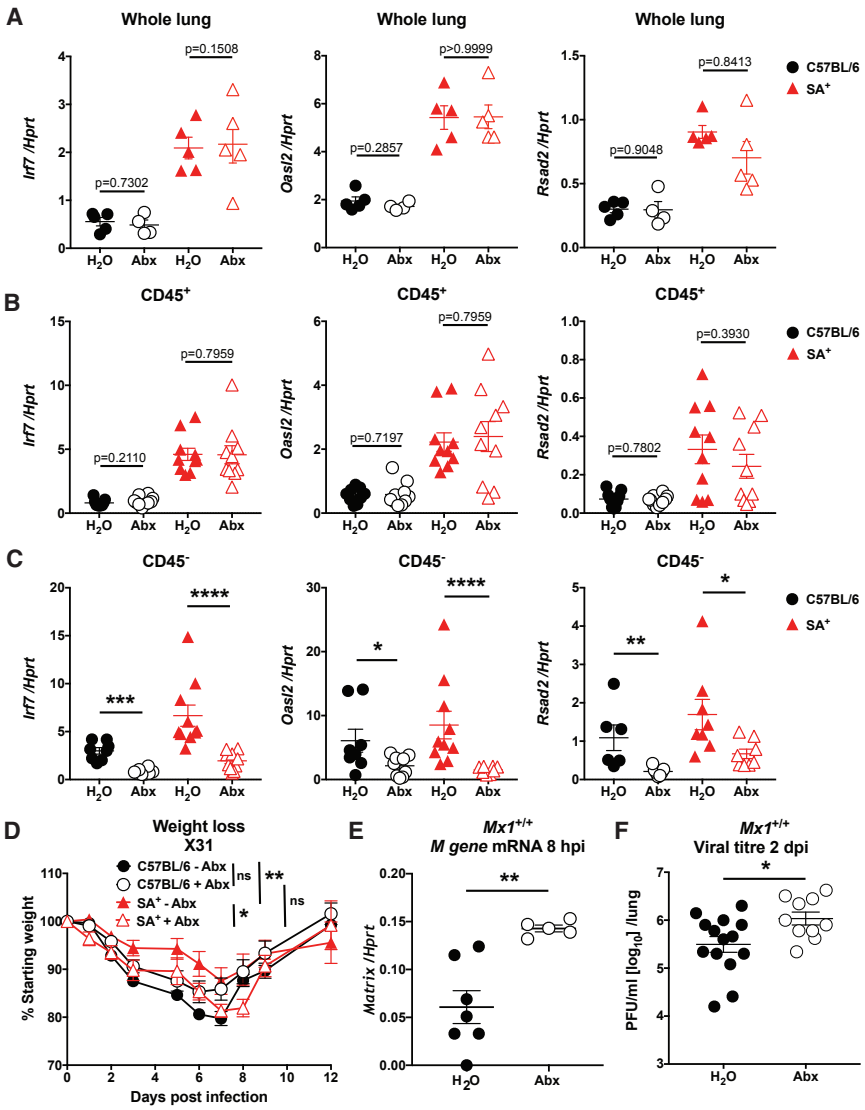

Figure 5. Reduced ISG Expression in Stromal Compartment of Antibiotic-Treated Mice Predisposes Them to Severe Influenza

(A) ISG expression of whole lungs from naive WT or *Ifnar1*^{SA} mice (n = 4 or 5 per group) given either plain water (closed symbols) or a cocktail of oral antibiotics (open symbols) for 4 weeks.

(B and C) Gene expression of MACS-sorted CD45^{+} (B) or CD45^{-} (C) cells from mice (n = 9 or 10 per group) as in (A).

(D) WT or *Ifnar1*^{SA} mice (n = 11 per group) given either plain water or antibiotics for 4 weeks prior to infection with 8,000 $TCID_{50}$ of X31. Mice were monitored for weight loss.

(E) *Mx1*$^{+/+}$ mice (n = 5–7 per group) were treated with antibiotics for 3 weeks and infected with 25,000 $TCID_{50}$ of hvPR8NS1(1–126) for 8 h. cDNA synthesized with oligo(dT) primers.

(F) *Mx1*$^{+/+}$ mice (n = 10–14 per group) were treated with antibiotics for 3 weeks and infected intranasally with 4 × 10^4 PFU of Udorn virus. After 48 h, lungs were harvested and virus titers determined by plaque assay on MDCK cells.

All qRT-PCR results shown are relative to the housekeeping gene *Hprt*. All bars represent mean ± SEM. Results are compiled from at least two experiments. Significance was determined using either 2-way ANOVA (D) or the Mann-Whitney U test (A–C, E, and F): *p < 0.05, **p < 0.01, ***p < 0.001, and ****p < 0.0001.

single amino acid residue in the IFNAR1 molecule (IFNAR1^{SA}), we also find that setting IFNAR1 surface levels is a mechanism constantly at work to fine-tune the baseline ISG signature. Using these mice for BM chimera experiments, we demonstrate the importance of stromal cell IFN signals for the early control of influenza virus load, while the immune cell compartment plays a role later during infection. Expression profiling of lung stroma from antibiotic-treated mice shows that microbiota maintain predominantly the IFN signature and additional immune-related pathways in these cells, and FT reverses the antibiotic-induced ISG reduction.

Previously, germ-free mice were shown to be more susceptible to influenza virus infection (Abt et al., 2012), but type I IFN-driven signals were not specifically assessed in those mice. Studies with antibiotic-treated mice (Abt et al., 2012; Ganal et al., 2012; Ichinohe et al., 2011; Oh et al., 2016; Steed et al., 2017) suggested that microbiota-driven viral resistance was linked to either increased IL-1β and IL18 transcript levels (Ichinohe et al., 2011) or to IFNα/β (Abt et al., 2012; Ganal et al., 2012; Steed et al., 2017). In these previous studies, the antiviral functions requiring a tonic IL-1β, IL-18, or IFN signal were identified in natural killer (NK) cells and macrophages. In addition, when antibiotic-treated mice were infected with a relatively low infectious dose of influenza virus, the adaptive immunity, including antibody, CD4, and CD8 responses, was reduced, leading to increases in virus levels on day 12 or 14 of infection (Abt et al., 2012; Ichinohe et al., 2011). Experiments in which lymphocytic choriomeningitis virus (LCMV) and murine cytomegalovirus (MCMV) inoculates were given systemically (Abt et al., 2012; Ganal et al., 2012) showed that microbiota enhanced immune cell activation. Therefore, effects on innate or adaptive immunity were implied in microbiota-driven antiviral resistance. Here we show that microbiota ablation affects the ISG signature in the lung most strongly in stromal cells, including epithelial cells, rather than in the immune cell compartment. In addition, the inverse correlation between the level of ISG and levels of viral transcription and replication at early time points, prior to IFN production and ISG induction by infection, indicates that microbiota-driven antiviral resistance precedes both adaptive immunity and innate immune cell function, and depends on the cell-intrinsic antiviral effects in the virus target cells, the lung epithelia. Together, this and previous studies demonstrate that microbiota-driven signals can act at multiple levels, inducing

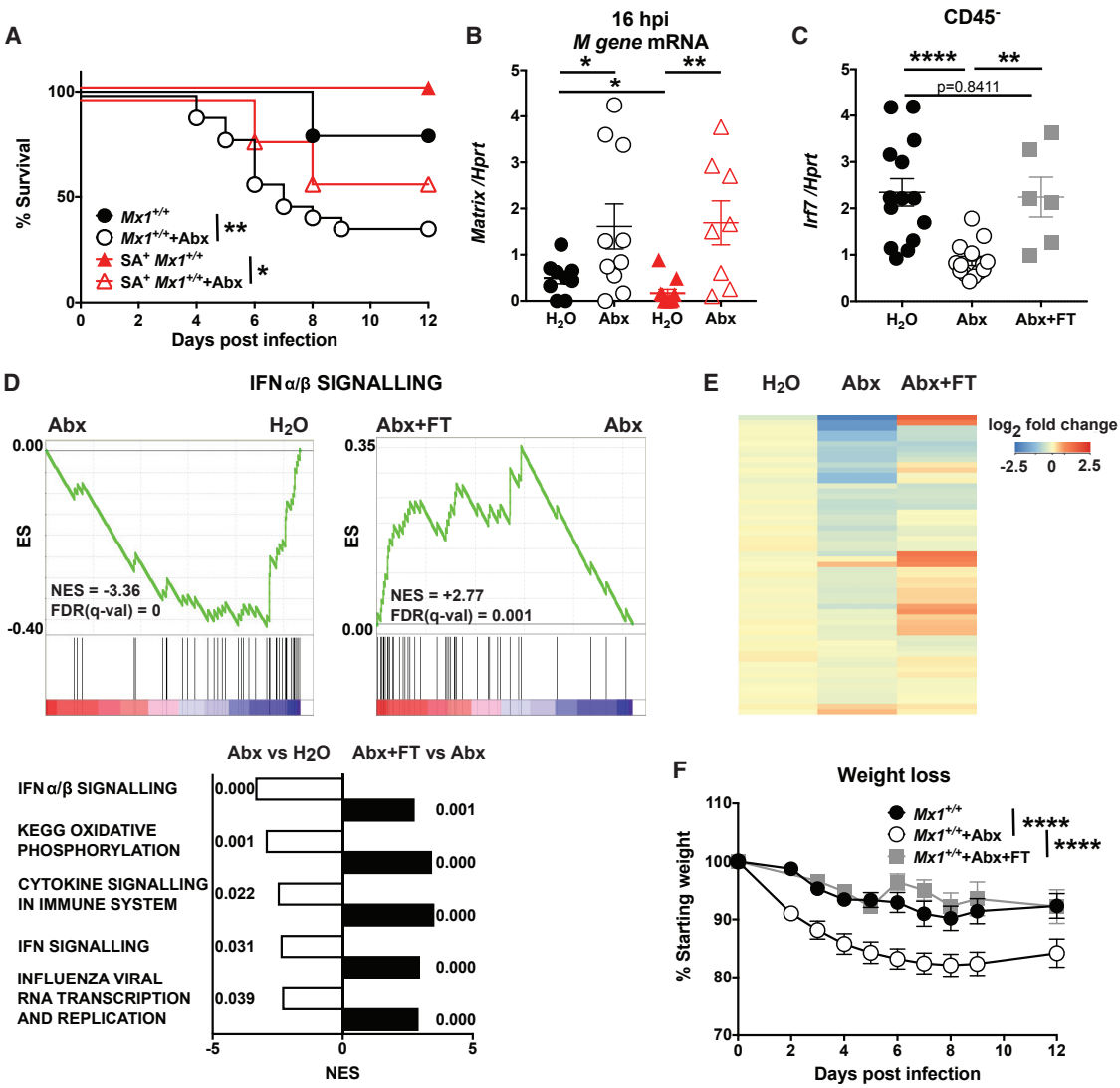

Figure 6. Microbiota Sustain Protective IFN-Driven Antiviral State in Lung Stroma

(A) *Mx1*$^{+/+}$ or *Mx1*$^{+/+}$*Ifnar1*^{SA} mice (n = 10–19 per group) were given either water or antibiotics for 4 weeks, prior to intranasal infection with 2,500 $TCID_{50}$ of hvPR8-NS1(1–126) virus. Mice were monitored for weight loss and survival.

(B) Mice (n = 8–11 per group) were infected as in (A) with 25,000 $TCID_{50}$ of hvPR8-NS1(1–126) virus and sacrificed 16 h post-infection. *M gene* expression was determined in MACS-sorted CD45^{-} cells. cDNA was generated using oligo(dT) primers.

(C) C57BL/6 mice (n = 6–14 per group) were treated as described in (A) or received antibiotics for 3 weeks and subsequently received two FTs 1 week prior to infection. CD45^{-} cells were MACS-purified from lungs, RNA prepared, and *Irf7* gene expression determined by qRT-PCR.

(D) RNA prepared as in (C) was used for RNA sequencing (RNA-seq) followed by gene set enrichment analysis (GSEA). Top panels show GSEA for the highest scoring gene set identified (IFNα/β signaling), with negative enrichment for the comparison Abx versus water and positive enrichment for Abx+FT versus Abx treatment. Bottom panel shows the normalized enrichment scores (NES) and false discovery rate (FDR) q-values (next to bars) for the highest scoring gene sets from the comparison (Abx versus water) that were also significantly changed in the comparison (Abx+FT versus Abx). n = 3 or 4 mice per group.

(E) Heatmap of expression of the genes contained in the gene sets "IFNα/β signaling" and "IFN signaling" pathways in the indicated treatment groups.

(F) *Mx1*$^{+/+}$ mice (n = 6–19 mice per group) were given either water or antibiotics for 4 weeks or antibiotics for 3 weeks followed by FT prior to intranasal infection with 2,500 $TCID_{50}$ of hvPR8-NS1(1–126) virus. Mice were monitored for weight loss.

All bars represent mean ± SEM. Results are compiled from at least two experiments. Significance was determined using the Gehan-Breslow-Wilcoxon test (A), unpaired t test (B), Mann-Whitney U test (C), or 2-way ANOVA (F): *p < 0.05, **p < 0.01, and ****p < 0.0001.

an antiviral state in non-immune cells at mucosal barriers to control infection early on, and enhancing the functionality of immune cells leading to improved innate and adaptive immunity later in infection.

We find that treatment with antibiotics reduces ISG expression mainly in stromal cells, but less so in hematopoietic cells, demonstrating that the main recipients of the microbiota-driven IFN signal are non-immune cells. A consequence of

this microbiota-dependent, pre-established ISG signature in epithelia is that already the earliest steps of influenza virus infection are blunted, with virus transcripts significantly reduced within the first 8 h of infection, and titers reduced by more than 5-fold within the first 2 days (Figures 5E and 5F). Subsequent antiviral immune responses are massively diminished because the virus stimulus itself is reduced early. This explains the apparent contradiction that *Ifnar1*^{SA} mice, which clearly have increased responses to IFN and show increased immune responses to inert stimuli (Figure S2G), show a less strong IFN response during viral infection compared with WT controls (Figures S2A and S2C). Importantly, this allows us to clearly identify the basis of enhanced protection in *Ifnar1*^{SA} mice. Because these mice have higher baseline ISGs but a weaker infection-induced IFN response, protection is due to the baseline effects, not to enhanced acute responses.

We show here that antibiotics treatment increases susceptibility in *Ifnar1*^{wt} mice that express the central influenza virus restriction factor *Mx1* (Figure 6A), which more closely resembles the presence of the homolog *MxA* in humans. In these mice, we observe early blunting of the infection, rather than enhanced (adaptive) immune responses later in infection as shown in previous studies. Most likely, the highly efficient Mx-driven intracellular antiviral response acts more rapidly and more directly and thus highlights the early effects of antibiotics treatment.

The exact origin and nature of the signal leading from microbiota to enhanced epithelial ISG signatures remain to be determined. Previous research has suggested that the microbiota-driven signal promoting an ISG signature in lung stromal cells could originate either from the gut or the lung. However, in the work presented here, the rescue of the phenotype by FT through oral gavage strongly suggests a gut involvement in this effect. Although a systemic impact of antibiotics treatment is documented, it is intriguing that in the lungs, immune cells which are presumably more exposed to systemic effects show less impact than epithelial cells, which could easily receive signals from bacteria in the airway lumen. It is also unknown whether the elevated ISG expression noted in the stromal compartment of the *Ifnar1*^{SA} mice is due to direct recognition of bacterial pathogen-associated molecular patterns by the lung epithelial cells or a response to IFNs produced by a lung-resident immune cell or a systemic source. We have tested and excluded pDCs as the cellular source of IFNα/β driving elevated set point ISG expression levels in *Ifnar1*^{SA} lungs (Figure 2G). Alternatively, lung-resident immune cells such as alveolar macrophages may produce a tonic IFNβ signal readily detectable by lung epithelial cells. Although our BM chimeras clearly indicate that the stroma genotype determines severity early in infection, we cannot formally exclude the possibility that a very early immune cell infiltrate also contributes to early virus control in *Ifnar1*^{SA} mice. This and the involvement of bacterial metabolites (Steed et al., 2017; Trompette et al., 2018) that act locally or systemically need to be investigated in the future.

Our study argues that caution should be exercised when treating patients with antibiotics. Between 2000 and 2015, worldwide antibiotic consumption is believed to have increased by 65%, much of which may be linked to inappropriate treatment of pollution- and viral-based illnesses (Klein et al., 2018). Our results suggest that inappropriate use of oral antibiotics could predispose patients to more severe influenza, because of reduced antiviral resistance of the epithelia.

We and others have shown previously that lung epithelia both produce and respond to type III IFN as well as type I IFN (Crotta et al., 2013). The data shown here suggest that the baseline ISG signature is not maintained by type III IFN, which would be produced in parallel to type I IFNs. These results are consistent with previous suggestions indicating an important role for IFNβ in maintaining tonic signaling (Erlandsson et al., 1998; Fleetwood et al., 2009; Gough et al., 2010, 2012; Takaoka et al., 2000; Thomas et al., 2006). We were not able to detect baseline tonic IFNα, IFNβ, IFNγ, or IFNλ protein expression in *Ifnar1*^{SA} or WT mice; however, strong upregulation of ISG expression in numerous cell types, including those not expressing type III IFN receptor, and the ablation of this signature by IFNα/β receptor-blocking monoclonal antibodies (mAbs), indicate that type I IFNs are present and active.

Interestingly, the strategy of elevated baseline ISGs is used by other tissues in the body to protect critical cell populations from infection. In the heart, elevated ISG baseline in cardiomyocytes protects this critical cell population, and cardiac fibroblasts express elevated levels of IFNAR1 on the surface, which make them more sensitive to IFNβ stimulation, preventing them from becoming a reservoir for viral infection (Zurney et al., 2007). Similar results have recently come to light regarding endothelial cells, in which IFITM3 is known to be constitutively expressed and helps prevent systemic spread and viral-mediated breakdown of the endothelial barrier by influenza virus (Sun et al., 2016; Tundup et al., 2017). Finally, hematopoietic stem cells also express elevated levels of ISGs, preventing infection from a wide range of viruses (Wu et al., 2018).

Given the enhanced protection conferred by increased IFNAR1 surface expression, the question arises as to why the IFN system is not physiologically tuned at a higher set point. Previous studies using *Ifnar1*^{SA} mice have shown that a range of inflammatory conditions are enhanced in these mice, indicating that a price must be paid for tuning up the IFN system constitutively (Bhattacharya et al., 2014). In the human population, it was shown for high-activity polymorphisms in the MDA5 gene that there is a trade-off between improved antiviral protection and increased inflammation (Cen et al., 2013; Crampton et al., 2012; Funabiki et al., 2014; Gorman et al., 2017). Use of the *Ifnar1*^{SA} mice allowed us to assess the role of IFNα/β receptor levels in setting the ISG baseline. We find that a slight elevation of IFNAR1 surface expression in *Ifnar1*^{SA} cells is enough to increase ISG expression in immune cells and the stromal compartment. This is clinically relevant because cells from individuals with Down syndrome, who carry an extra copy of the *Ifnar1/2* genes on chromosome 21, have been shown to express elevated IFNAR1 surface levels. Blood cells from these individuals produce increased amounts of proinflammatory cytokines in response to virus, and recent studies (Sullivan et al., 2016) have found an enhanced blood ISG signature in Down syndrome patients. Changes in blood proteomics of Down syndrome individuals resemble those found in type I interferonopathies and other autoinflammatory conditions (Sullivan et al., 2017). Using *Ifnar1*^{SA} mice, we demonstrate here that fine-tuning surface

IFNAR1 levels is critical to balance the antiviral and proinflammatory properties of the IFN system.

STAR★METHODS

Detailed methods are provided in the online version of this paper and include the following:

- KEY RESOURCES TABLE
- LEAD CONTACT AND MATERIALS AVAILABILITY
- EXPERIMENTAL MODEL AND SUBJECT DETAILS
  - Mice and treatments
  - Viruses, titers, and cells
- METHOD DETAILS
  - ISG expression in mice
  - Viral infection, interferon and poly I:C stimulation of mice
  - Depletion and blockade by antibodies
  - Differentiation of bone marrow derived cells and primary mouse tracheal epithelial cell culture (mTEC)
  - CD45 isolation from lung tissue
  - RNaseq
  - Flow cytometry analysis
  - Protein analysis
- QUANTIFICATION AND STATISTICAL ANALYSIS
- DATA AND CODE AVAILABILITY

SUPPLEMENTAL INFORMATION

Supplemental Information can be found online at https://doi.org/10.1016/j.celrep.2019.05.105.

ACKNOWLEDGMENTS

We would like to thank J. Rappe, M. Stankovic, M. Wilson, L. Entwistle, L. Parker, and J. McCauley for reagents and advice on this project and manuscript. We would also like to thank the following Science Technology Platforms—Advanced Sequencing and Bioinformatics, Biological Research Facility, and Bioinformatics at the Francis Crick Institute, as well as the National Institute for Medical Research at Mill Hill—for their critical support throughout the project. This study was supported by the Francis Crick Institute, which receives its core funding from Cancer Research UK (FC001206), the UK Medical Research Council (MRC) (FC001206), and the Wellcome Trust (FC001206). Support by MRC grant U117597139 (K.C.B., S.C., S.D., A.W.) and Deutsche Forschungsgemeinschaft grant SFB 1160 (D.S., P.S.) is gratefully acknowledged.

AUTHOR CONTRIBUTIONS

A.W. and K.C.B. designed the study. K.C.B., K.F., D.S., S.D., S.C., and P.S. designed and performed the experiments. K.C.B., K.F., M.L., A.W., P.S., S.C., and D.S. analyzed and interpreted results. K.C.B., K.F., S.C., and A.W. wrote the paper. P.S. and S.Y.F. provided novel mouse strains. All authors helped finalize the paper.

DECLARATION OF INTERESTS

The authors declare no conflicts of interest.

Received: August 2, 2018
Revised: May 10, 2019
Accepted: May 29, 2019
Published: July 2, 2019

REFERENCES

Abt, M.C., Osborne, L.C., Monticelli, L.A., Doering, T.A., Alenghat, T., Sonnenberg, G.F., Paley, M.A., Antenus, M., Williams, K.L., Erikson, J., et al. (2012). Commensal bacteria calibrate the activation threshold of innate antiviral immunity. Immunity *37*, 158–170.

Bergmann, M., García-Sastre, A., Carnero, E., Pehamberger, H., Wolff, K., Palese, P., and Muster, T. (2000). Influenza virus NS1 protein counteracts PKR-mediated inhibition of replication. J. Virol. *74*, 6203–6206.

Bhattacharya, S., Katlinski, K.V., Reichert, M., Takano, S., Brice, A., Zhao, B., Yu, Q., Zheng, H., Carbone, C.J., Katlinskaya, Y.V., et al. (2014). Triggering ubiquitination of IFNAR1 protects tissues from inflammatory injury. EMBO Mol. Med. *6*, 384–397.

Bosinger, S.E., and Utay, N.S. (2015). Type I interferon: understanding its role in HIV pathogenesis and therapy. Curr. HIV/AIDS Rep. *12*, 41–53.

Cen, H., Wang, W., Leng, R.-X., Wang, T.-Y., Pan, H.-F., Fan, Y.-G., Wang, B., and Ye, D.-Q. (2013). Association of IFIH1 rs1990760 polymorphism with susceptibility to autoimmune diseases: a meta-analysis. Autoimmunity *46*, 455–462.

Chen, Z., Li, Y., and Krug, R.M. (1999). Influenza A virus NS1 protein targets poly(A)-binding protein II of the cellular 3′-end processing machinery. EMBO J. *18*, 2273–2283.

Crampton, S.P., Deane, J.A., Feigenbaum, L., and Bolland, S. (2012). Ifih1 gene dose effect reveals MDA5-mediated chronic type I IFN gene signature, viral resistance, and accelerated autoimmunity. J. Immunol. *188*, 1451–1459.

Crotta, S., Davidson, S., Mahlakoiv, T., Desmet, C.J., Buckwalter, M.R., Albert, M.L., Staeheli, P., and Wack, A. (2013). Type I and type III interferons drive redundant amplification loops to induce a transcriptional signature in influenza-infected airway epithelia. PLoS Pathog. *9*, e1003773.

Davidson, S., Crotta, S., McCabe, T.M., and Wack, A. (2014). Pathogenic potential of interferon αβ in acute influenza infection. Nat. Commun. *5*, 3864.

Deeg, C.M., Hassan, E., Mutz, P., Rheinemann, L., Götz, V., Magar, L., Schilling, M., Kallfass, C., Nürnberger, C., Soubies, S., et al. (2017). In vivo evasion of MxA by avian influenza viruses requires human signature in the viral nucleoprotein. J. Exp. Med. *214*, 1239–1248.

Egorov, A., Brandt, S., Sereinig, S., Romanova, J., Ferko, B., Katinger, D., Grassauer, A., Alexandrova, G., Katinger, H., and Muster, T. (1998). Transfectant influenza A viruses with long deletions in the NS1 protein grow efficiently in Vero cells. J. Virol. *72*, 6437–6441.

Erlandsson, L., Blumenthal, R., Eloranta, M.L., Engel, H., Alm, G., Weiss, S., and Leanderson, T. (1998). Interferon-beta is required for interferon-alpha production in mouse fibroblasts. Curr. Biol. *8*, 223–226.

Finter, N.B., Chapman, S., Dowd, P., Johnston, J.M., Manna, V., Sarantis, N., Sheron, N., Scott, G., Phua, S., and Tatum, P.B. (1991). The use of interferon-alpha in virus infections. Drugs *42*, 749–765.

Fleetwood, A.J., Dinh, H., Cook, A.D., Hertzog, P.J., and Hamilton, J.A. (2009). GM-CSF- and M-CSF-dependent macrophage phenotypes display differential dependence on type I interferon signaling. J. Leukoc. Biol. *86*, 411–421.

François-Newton, V., Magno de Freitas Almeida, G., Payelle-Brogard, B., Monneron, D., Pichard-Garcia, L., Piehler, J., Pellegrini, S., and Uzé, G. (2011). USP18-based negative feedback control is induced by type I and type III interferons and specifically inactivates interferon α response. PLoS ONE *6*, e22200.

Funabiki, M., Kato, H., Miyachi, Y., Toki, H., Motegi, H., Inoue, M., Minowa, O., Yoshida, A., Deguchi, K., Sato, H., et al. (2014). Autoimmune disorders associated with gain of function of the intracellular sensor MDA5. Immunity *40*, 199–212.

Ganal, S.C., Sanos, S.L., Kallfass, C., Oberle, K., Johner, C., Kirschning, C., Lienenklaus, S., Weiss, S., Staeheli, P., Aichele, P., and Diefenbach, A. (2012). Priming of natural killer cells by nonmucosal mononuclear phagocytes requires instructive signals from commensal microbiota. Immunity *37*, 171–186.

García-Sastre, A. (2011). Induction and evasion of type I interferon responses by influenza viruses. Virus Res. *162*, 12–18.

García-Sastre, A., and Biron, C.A. (2006). Type 1 interferons and the virus-host relationship: a lesson in détente. Science *312*, 879–882.

García-Sastre, A., Egorov, A., Matassov, D., Brandt, S., Levy, D.E., Durbin, J.E., Palese, P., and Muster, T. (1998). Influenza A virus lacking the NS1 gene replicates in interferon-deficient systems. Virology *252*, 324–330.

Gorman, J.A., Hundhausen, C., Errett, J.S., Stone, A.E., Allenspach, E.J., Ge, Y., Arkatkar, T., Clough, C., Dai, X., Khim, S., et al. (2017). The A946T variant of the RNA sensor IFIH1 mediates an interferon program that limits viral infection but increases the risk for autoimmunity. Nat. Immunol. *18*, 744–752.

Gougeon, M.L., and Herbeuval, J.P. (2012). IFN-α and TRAIL: a double edge sword in HIV-1 disease? Exp. Cell Res. *318*, 1260–1268.

Gough, D.J., Messina, N.L., Hii, L., Gould, J.A., Sabapathy, K., Robertson, A.P.S., Trapani, J.A., Levy, D.E., Hertzog, P.J., Clarke, C.J.P., and Johnstone, R.W. (2010). Functional crosstalk between type I and II interferon through the regulated expression of STAT1. PLoS Biol. *8*, e1000361–e1000312.

Gough, D.J., Messina, N.L., Clarke, C.J.P., Johnstone, R.W., and Levy, D.E. (2012). Constitutive type I interferon modulates homeostatic balance through tonic signaling. Immunity *36*, 166–174.

Goulding, J., Godlee, A., Vekaria, S., Hilty, M., Snelgrove, R., and Hussell, T. (2011). Lowering the threshold of lung innate immune cell activation alters susceptibility to secondary bacterial superinfection. J. Infect. Dis. *204*, 1086–1094.

Gracias, D.T., Stelekati, E., Hope, J.L., Boesteanu, A.C., Doering, T.A., Norton, J., Mueller, Y.M., Fraietta, J.A., Wherry, E.J., Turner, M., and Katsikis, P.D. (2013). The microRNA miR-155 controls CD8(+) T cell responses by regulating interferon signaling. Nat. Immunol. *14*, 593–602.

Huangfu, W.C., Qian, J., Liu, C., Liu, J., Lokshin, A.E., Baker, D.P., Rui, H., and Fuchs, S.Y. (2012). Inflammatory signaling compromises cell responses to interferon alpha. Oncogene *31*, 161–172.

Ichinohe, T., Pang, I.K., Kumamoto, Y., Peaper, D.R., Ho, J.H., Murray, T.S., and Iwasaki, A. (2011). Microbiota regulates immune defense against respiratory tract influenza A virus infection. Proc. Natl. Acad. Sci. U S A *108*, 5354–5359.

Isaacs, A., and Lindenmann, J. (1957). Virus interference. I. The interferon. Proc. R. Soc. Lond. B Biol. Sci. *147*, 258–267.

Jacquelin, B., Mayau, V., Targat, B., Liovat, A.S., Kunkel, D., Petitjean, G., Dillies, M.A., Roques, P., Butor, C., Silvestri, G., et al. (2009). Nonpathogenic SIV infection of African green monkeys induces a strong but rapidly controlled type I IFN response. J. Clin. Invest. *119*, 3544–3555.

Kadowaki, N., Antonenko, S., Lau, J.Y., and Liu, Y.J. (2000). Natural interferon alpha/beta-producing cells link innate and adaptive immunity. J. Exp. Med. *192*, 219–226.

Kawashima, T., Kosaka, A., Yan, H., Guo, Z., Uchiyama, R., Fukui, R., Kaneko, D., Kumagai, Y., You, D.-J., Carreras, J., et al. (2013). Double-stranded RNA of intestinal commensal but not pathogenic bacteria triggers production of protective interferon-β. Immunity *38*, 1187–1197.

Klein, E.Y., Van Boeckel, T.P., Martinez, E.M., Pant, S., Gandra, S., Levin, S.A., Goossens, H., and Laxminarayan, R. (2018). Global increase and geographic convergence in antibiotic consumption between 2000 and 2015. Proc. Natl. Acad. Sci. U S A *115*, E3463–E3470.

Klinkhammer, J., Schnepf, D., Ye, L., Schwaderlapp, M., Gad, H.H., Hartmann, R., Garcin, D., Mahlakõiv, T., and Staeheli, P. (2018). IFN-λ prevents influenza virus spread from the upper airways to the lungs and limits virus transmission. eLife *7*, 7.

Kochs, G., Martínez-Sobrido, L., Lienenklaus, S., Weiss, S., García-Sastre, A., and Staeheli, P. (2009). Strong interferon-inducing capacity of a highly virulent variant of influenza A virus strain PR8 with deletions in the NS1 gene. J. Gen. Virol. *90*, 2990–2994.

Kristiansen, H., Gad, H.H., Eskildsen-Larsen, S., Despres, P., and Hartmann, R. (2011). The oligoadenylate synthetase family: an ancient protein family with multiple antiviral activities. J. Interferon Cytokine Res. *31*, 41–47.

Lee-Kirsch, M.A., Gong, M., Chowdhury, D., Senenko, L., Engel, K., Lee, Y.-A., de Silva, U., Bailey, S.L., Witte, T., Vyse, T.J., et al. (2007). Mutations in the gene encoding the 3′-5′ DNA exonuclease TREX1 are associated with systemic lupus erythematosus. Nat. Genet. *39*, 1065–1067.

Levin, D., Harari, D., and Schreiber, G. (2011). Stochastic receptor expression determines cell fate upon interferon treatment. Mol. Cell. Biol. *31*, 3252–3266.

Li, H., Bradley, K.C., Long, J.S., Frise, R., Ashcroft, J.W., Hartgroves, L.C., Shelton, H., Makris, S., Johansson, C., Cao, B., and Barclay, W.S. (2018). Internal genes of a highly pathogenic H5N1 influenza virus determine high viral replication in myeloid cells and severe outcome of infection in mice. PLoS Pathog. *14*, e1006821–e1006825.

Liu, J., HuangFu, W.C., Kumar, K.G., Qian, J., Casey, J.P., Hamanaka, R.B., Grigoriadou, C., Aldabe, R., Diehl, J.A., and Fuchs, S.Y. (2009). Virus-induced unfolded protein response attenuates antiviral defenses via phosphorylation-dependent degradation of the type I interferon receptor. Cell Host Microbe *5*, 72–83.

Moraga, I., Harari, D., Schreiber, G., Uzé, G., and Pellegrini, S. (2009). Receptor density is key to the alpha2/beta interferon differential activities. Mol. Cell. Biol. *29*, 4778–4787.

Mordstein, M., Kochs, G., Dumoutier, L., Renauld, J.C., Paludan, S.R., Klucher, K., and Staeheli, P. (2008). Interferon-lambda contributes to innate immunity of mice against influenza A virus but not against hepatotropic viruses. PLoS Pathog. *4*, e1000151.

Oh, J.E., Kim, B.-C., Chang, D.-H., Kwon, M., Lee, S.Y., Kang, D., Kim, J.Y., Hwang, I., Yu, J.-W., Nakae, S., and Lee, H.K. (2016). Dysbiosis-induced IL-33 contributes to impaired antiviral immunity in the genital mucosa. Proc. Natl. Acad. Sci. U S A *113*, E762–E771.

Pavlovic, J., Haller, O., and Staeheli, P. (1992). Human and mouse Mx proteins inhibit different steps of the influenza virus multiplication cycle. J. Virol. *66*, 2564–2569.

Qian, J., Zheng, H., Huangfu, W.C., Liu, J., Carbone, C.J., Leu, N.A., Baker, D.P., and Fuchs, S.Y. (2011). Pathogen recognition receptor signaling accelerates phosphorylation-dependent degradation of IFNAR1. PLoS Pathog. *7*, e1002065.

Rajsbaum, R., Albrecht, R.A., Wang, M.K., Maharaj, N.P., Versteeg, G.A., Nistal-Villán, E., García-Sastre, A., and Gack, M.U. (2012). Species-specific inhibition of RIG-I ubiquitination and IFN induction by the influenza A virus NS1 protein. PLoS Pathog. *8*, e1003059.

Reed, L.J., and Muench, H. (1938). A simple method of estimating fifty per cent endpoints. Am. J. Epidemiol. *27*, 493–497.

Steed, A.L., Christophi, G.P., Kaiko, G.E., Sun, L., Goodwin, V.M., Jain, U., Esaulova, E., Artyomov, M.N., Morales, D.J., Holtzman, M.J., et al. (2017). The microbial metabolite desaminotyrosine protects from influenza through type I interferon. Science *357*, 498–502.

Stifter, S.A., and Feng, C.G. (2015). Interfering with immunity: detrimental role of type I IFNs during infection. J. Immunol. *194*, 2455–2465.

Sullivan, K.D., Lewis, H.C., Hill, A.A., Pandey, A., Jackson, L.P., Cabral, J.M., Smith, K.P., Liggett, L.A., Gomez, E.B., Galbraith, M.D., et al. (2016). Trisomy 21 consistently activates the interferon response. eLife *5*, e16220.

Sullivan, K.D., Evans, D., Pandey, A., Hraha, T.H., Smith, K.P., Markham, N., Rachubinski, A.L., Wolter-Warmerdam, K., Hickey, F., Espinosa, J.M., and Blumenthal, T. (2017). Trisomy 21 causes changes in the circulating proteome indicative of chronic autoinflammation. Sci. Rep. *7*, 14818.

Sun, X., Zeng, H., Kumar, A., Belser, J.A., Maines, T.R., and Tumpey, T.M. (2016). Constitutively expressed IFITM3 protein in human endothelial cells poses an early infection block to human influenza viruses. J. Virol. *90*, 11157–11167.

Takaoka, A., Mitani, Y., Suemori, H., Sato, M., Yokochi, T., Noguchi, S., Tanaka, N., and Taniguchi, T. (2000). Cross talk between interferon-gamma and -alpha/beta signaling components in caveolar membrane domains. Science *288*, 2357–2360.

Teijaro, J.R., Ng, C., Lee, A.M., Sullivan, B.M., Sheehan, K.C.F., Welch, M., Schreiber, R.D., de la Torre, J.C., and Oldstone, M.B.A. (2013). Persistent

LCMV infection is controlled by blockade of type I interferon signaling. Science *340*, 207–211.

Thomas, K.E., Galligan, C.L., Newman, R.D., Fish, E.N., and Vogel, S.N. (2006). Contribution of interferon-beta to the murine macrophage response to the toll-like receptor 4 agonist, lipopolysaccharide. J. Biol. Chem. *281*, 31119–31130.

Trompette, A., Gollwitzer, E.S., Pattaroni, C., Lopez-Mejia, I.C., Riva, E., Pernot, J., Ubags, N., Fajas, L., Nicod, L.P., and Marsland, B.J. (2018). Dietary fiber confers protection against flu by shaping Ly6c(-) patrolling monocyte hematopoiesis and CD8(+) T cell metabolism. Immunity *48*, 992–1005.e8.

Tundup, S., Kandasamy, M., Perez, J.T., Mena, N., Steel, J., Nagy, T., Albrecht, R.A., and Manicassamy, B. (2017). Endothelial cell tropism is a determinant of H5N1 pathogenesis in mammalian species. PLoS Pathog. *13*, e1006270.

Utay, N.S., and Douek, D.C. (2016). Interferons and HIV infection: the good, the bad, and the ugly. Pathog. Immun. *1*, 107–116.

Versteeg, G.A., and García-Sastre, A. (2010). Viral tricks to grid-lock the type I interferon system. Curr. Opin. Microbiol. *13*, 508–516.

Ward, C.L., Dempsey, M.H., Ring, C.J., Kempson, R.E., Zhang, L., Gor, D., Snowden, B.W., and Tisdale, M. (2004). Design and performance testing of quantitative real time PCR assays for influenza A and B viral load measurement. J. Clin. Virol. *29*, 179–188.

Wilson, E.B., Yamada, D.H., Elsaesser, H., Herskovitz, J., Deng, J., Cheng, G., Aronow, B.J., Karp, C.L., and Brooks, D.G. (2013). Blockade of chronic type I interferon signaling to control persistent LCMV infection. Science *340*, 202–207.

Wu, X., Dao Thi, V.L., Huang, Y., Billerbeck, E., Saha, D., Hoffmann, H.-H., Wang, Y., Silva, L.A.V., Sarbanes, S., Sun, T., et al. (2018). Intrinsic immunity shapes viral resistance of stem cells. Cell *172*, 423–438.e25.

Xia, C., Vijayan, M., Pritzl, C.J., Fuchs, S.Y., McDermott, A.B., and Hahm, B. (2015). Hemagglutinin of influenza A virus antagonizes type I IFN responses by inducing degradation of type I IFN receptor 1. J. Virol. *90*, 2403–2417.

Yoshimura, A., Naka, T., and Kubo, M. (2007). SOCS proteins, cytokine signalling and immune regulation. Nat. Rev. Immunol. *7*, 454–465.

You, Y., Richer, E.J., Huang, T., and Brody, S.L. (2002). Growth and differentiation of mouse tracheal epithelial cells: selection of a proliferative population. Am. J. Physiol. Lung Cell. Mol. Physiol. *283*, L1315–L1321.

Zheng, H., Qian, J., Carbone, C.J., Leu, N.A., Baker, D.P., and Fuchs, S.Y. (2011). Vascular endothelial growth factor-induced elimination of the type 1 interferon receptor is required for efficient angiogenesis. Blood *118*, 4003–4006.

Zurney, J., Howard, K.E., and Sherry, B. (2007). Basal expression levels of IFNAR and Jak-STAT components are determinants of cell-type-specific differences in cardiac antiviral responses. J. Virol. *81*, 13668–13680.

STAR★METHODS

KEY RESOURCES TABLE

REAGENT or RESOURCE	SOURCE	IDENTIFIER
Antibodies		
Anti-CD3 Fitc (Clone: 17A2)	eBioscience	Cat#14-0032-82
Anti-CD4 BV605 (Clone: Rm4-5)	Biolegend	Cat#100548
Anti-CD8a BV510 (Clone: 53-6.7)	Biolegend	Cat#100752
Anti-CD11b PE Cy7 (Clone: M1/70)	Biolegend	Cat#101216
Anti-CD11c BV421 (Clone: N418)	Biolegend	Cat#117343
Anti-CD19 PE Cy7 (Clone: 6D5)	Biolegend	Cat#115520
Anti-CD31 BV421 (Clone: MBC78.2)	Invitrogen	Cat#RM5228
Anti-CD44 PE (Clone: IM7)	eBioscience	Cat#15228539
Anti-CD45 APC (Clone: 30-F11)	Biolegend	Cat#103112
Anti-CD64 APC (Clone: X54-5/7.1)	Biolegend	Cat#139306
Anti-CD69 BV421 (Clone: H1-2F3)	Biolegend	Cat#104545
Anti-CD200R (Clone: OX-110)	Biorad	Cat#MCA2281
Anti-Ecadherin FITC (Clone: 36)	BD Biosciences	Cat#612131
Anti-EPCAM BV605 (Clone: 9C4)	Biolegend	Cat#324224
Anti-IFNAR1 PE (Clone: MAR1-5A3)	Biolegend	Cat#127312
Anti-Ly6C BV605 (Clone: HK1.4)	Biolegend	Cat#128036
Anti-Ly6G FITC (Clone: 1A8)	Biolegend	Cat#127606
Anti-MARCO FITC (Clone: ED31)	Biorad	Cat#MCA1849
Anti-MHCII BV711 (Clone: M5/114.15.2)	Biolegend	Cat#107643
Anti-NKp46 APC (Clone: 29A1.4)	Biolegend	Cat#137608
Anti-PDCA1 FITC (Clone: 927)	Biolegend	Cat#127008
Anti-Sca1 BV711 (Clone: D7)	Biolegend	Cat#108131
Anti-Siglec F APC Cy7 (Clone: E50-2440)	BD bioscience	Cat#565527
Anti-Siglec H PE (Clone: 551)	Biolegend	Cat#129606
CD45 MicroBeads, mouse	Miltenyi	Cat#130-052-301
Fixable blue dead stain (BUV395)	Thermo Fisher	Cat#L23105
InVivoMab anti-mouse IFNAR-1 (MAR1-5A3)	Bio X cell	Cat#BE0241
InVivoMab anti-mouse PDCA1 (Clone: 927)	Bio X Cell	Cat#BE0311
Bacterial and Virus Strains		
hvPR8-NS1(1-126)	Wack Lab	Kochs et al., 2009
PR8	Wack Lab	Dr J. Skehel, FCI-MH
Udorn	Staeheli Lab	Klinkhammer et al., 2018
X31	Wack Lab	Dr J. Skehel, FCI-MH
Chemicals, Peptides, and Recombinant Proteins		
Ampicillin trihydrate	Sigma-Aldrich	Cat#A6140
DNase I from bovine pancreas	Sigma-Aldrich	Cat#D4527
Gentamycin sulfate salt	Sigma-Aldrich	Cat#G3632
Liberase TL	Roche	Cat#54010200001
Metronidazole	Sigma-Aldrich	Cat#M3761
Mouse IFNα_4	PBL	Cat#12115-1
Plasmocin treatment	InvivoGen	Cat#ant-mpt
polyI:C	InvivoGen	Cat#tlrl-pic
Trypsin from bovine pancreas	Sigma	Cat#T1426
Vancomycin hydrochloride	Sigma	Cat#SBR00001

(*Continued on next page*)

Continued

REAGENT or RESOURCE	SOURCE	IDENTIFIER
Critical Commercial Assays		
Cytokine & Chemokine 36-Plex Mouse ProcartaPlex Panel 1A	Invtrogen	Cat#EPX360-26092-901
IFNα/β 2-Plex Mouse ProcartaPlex Panel	Invitrogen	Cat#EPX020-22187-901
Mouse IL-28B/IFNλ$_3$ DuoSet ELISA	R&D	Cat#DY1789B
Ovation RNA-Seq System V2	NuGen	Cat#7102-08
Ovation Ultralow System V2	NuGen	Cat#0344
qPCRBIO cDNA Synthesis Kit	PCR Biosystems	Cat#: PB30.11-02
qPCRBIO Probe Mix	PCR Biosystems	Cat#: PB20.21-01
QuantiTect Reverse Transcription Kit	QIAGEN	Cat#205310
RNeasy Micro Kit	QIAGEN	Cat#74004
RNeasy Mini Kit	QIAGEN	Cat#74104
Deposited Data		
Raw and analyzed data	This paper	GEO: GSE129073
Experimental Models: Cell Lines		
MDCK	Francis Crick Institute	n/a
Experimental Models: Organisms/Strains		
C57BL/6J	MRC-NIMR/Francis Crick Institute	n/a
Ifnar1^{SA}	MRC-NIMR/Francis Crick Institute	Zheng et al., 2011
Mx1$^{+/+}$ (B6.A2G-Mx1)	MRC-NIMR/Francis Crick Institute	Mordstein et al., 2008
Mx1$^{+/+}$ Ifnar1^{SA}	MRC-NIMR/Francis Crick Institute	n/a
MxA$^{tg/tg}$	University of Freiburg	Deeg et al., 2017
MxA$^{tg/tg}$ Ifnar1^{SA}	University of Freiburg	n/a
Oligonucleotides		
Hprt (mm00446968_m1)	Thermo Fisher	Cat#4331182
Ifna4 (Mm00833969_s1)	Thermo Fisher	Cat#4331182
Ifnb1 (mm0439552_s1)	Thermo Fisher	Cat#4331182
Ifng (Mm01168134_m1)	Thermo Fisher	Cat#4331182
Ifnl2/3 (mm04204156_gh)	Thermo Fisher	Cat#4331182
Irf7 (mm05516791_g1)	Thermo Fisher	Cat#4331182
Oasl2 (mm0496187_m1)	Thermo Fisher	Cat#4331182
Rsad2 (mm00491265_m1)	Thermo Fisher	Cat#4331182
Stat1 (mm0439531_m1)	Thermo Fisher	Cat#4331182
PR8 sense (5′ -AAGACCAATCCTGTCACCTCTGA- 3′)	Sigma-Aldrich	Ward et al., 2004
PR8 anti-sense (5′ -CAAAGCGTCTACGCTGCAGTCC- 3′)	Sigma-Aldrich	Ward et al., 2004
PR8 Probe (FAM - 5′ – TTTGTGTTCACGCT CACCGT –3′ - TAMRA)	Sigma-Aldrich	Ward et al., 2004
Software and Algorithms		
FlowJo	Treestar	v10.3
Prism 7	GraphPad	v7.0c
QuantStudio Design & Analysis	appliedbiosystems	v1.4

LEAD CONTACT AND MATERIALS AVAILABILITY

Further information and requests for resources and reagents should be directed to and will be fulfilled by the Lead Contact, Andreas Wack (andreas.wack@crick.ac.uk).

EXPERIMENTAL MODEL AND SUBJECT DETAILS

Mice and treatments

All mouse strains including *Ifnar1*$^{+/+}$ (wild-type), *Ifnar1*$^{-/-}$ and *Ifnar1*^{SA} (Bhattacharya et al., 2014; Zheng et al., 2011) are on the C57BL/6J background and were bred at either MRC-NIMR or the Francis Crick Institute under specific pathogen free conditions.

All protocols for breeding and experiments were approved by internal ethics committees at the Francis Crick Institute as well as the MRC-NIMR. All experiments were a part of the project license approved by the Home Office, UK, under the Animals (Scientific Procedures) Act 1986. *MxA*$^{tg/tg}$ mice were generated as previously described (Deeg et al., 2017), and these mice were crossed to *Ifnar1*^{SA} mice to generate the *MxA*$^{tg/tg}$ *Ifnar1*^{SA} mouse line on the C57BL/6J background. Both colonies were maintained in specific pathogen free conditions at the University of Freiburg. For co-housing procedures, two cages of 6-8 week old female *Ifnar1*^{SA} and wild-type mice were co-housed for four weeks prior to determination of lung baseline ISG expression. Antibiotics-treated mice were given the following cocktail for 3-4 weeks: 100 mg ampicillin, 100 mg vancomycin, 100 mg metronidazole, and 100 mg gentamicin in 100 ml water (changed twice a week). For fecal transplants, two fecal pellets from the control group were homogenized in 1 ml PBS, and 200 μl volume were gavaged orally. Gavage occurred twice (on day 2 and day 5) post antibiotics treatment and then animals were infected with influenza virus on day 7 post-antibiotics treatment (Steed et al., 2017).

Viruses, titers, and cells

Influenza A viruses X31, PR8, and hvPR8-NS1(1-126) (Kochs et al., 2009) were grown in eggs and filtered (0.2 μm) prior to titration. All virus stocks were tested for contaminants by overnight incubation in LB media, as well as for standard pathogens by microbiological services facility at the Francis Crick Institute. $TCID_{50}$ determined by plating MDCK cells overnight on a 48 well plate in DMEM + 10% FCS + 1% Penicillin/Streptomycin. When cells reached 75%–80% confluency, plates were washed, and 4-6 replicates of virus were serially diluted 1:10 in 250 μl total volume. Inoculum was left for 1 hour at 37°C, aspirated, and replaced with serum free DMEM + 1% Penicillin/Streptomycin + 0.5 μg/ml TPCK trypsin. Cells incubated at 37°C for 2-3 days. Infected cells were then washed with PBS prior to incubation with 200 μl of 0.25% turkey red blood cells (A kind gift from Professor John McCauley and Public Health England) for 1 hour at 4°C. Plates were thoroughly washed with cold PBS, and analyzed for positivity either by clearance of cells, or turkey red blood cell binding. Calculations to determine $TCID_{50}$ carried out using the Reed and Muench methodology (Reed and Muench, 1938). MDCK cells were maintained in DMEM + 1% Penicillin/Streptomycin + 10% FCS. During maintenance passages, a prophylactic dose of Plasmosin was included in the media at 2.5 mg/ml to prevent contamination with mycoplasma.

METHOD DETAILS

ISG expression in mice

Mice from six different colonies were examined for expression of ISGs. Lungs were harvested and stored in RNALater at either −80°C for long term storage or −20°C until homogenized with a Kinematica Polytron PT 10-35 homogenizer in 3 ml RLT buffer (QIAGEN) + β-mercaptoethanol. 600 μl of homogenized lung tissue was used to isolate RNA using the RNeasy Mini Kit or RNeasy Micro Kit ($CD45^-$ cells). cDNA was created either using the QuantiTect Reverse Transcription Kit with oligo(dT) primers or by using random hexamer primers using qPCRBIO cDNA synthesis kit as per manufacturer's instructions. RT-qPCR was performed on an Applied Biosystems Quantstudio 3 RT-qPCR machine with 1x qPCRBIO Probe Mix Lo-ROX, and 1x taqman primers. Levels of RNA were normalized prior to cDNA synthesis. Results were normalized to the housekeeping gene *Hprt*. Lung RNA samples processed from *MxA*$^{tg/tg}$ and *Ifnar1*^{SA}*MxA*$^{tg/tg}$ were collected in Trizol prior to homogenization and RNA purified using RNeasy columns.

Viral infection, interferon and poly I:C stimulation of mice

For inert intranasal viral stimulus, 6-10 weeks old C57BL/6 and *Ifnar1*^{SA} mice were anesthetised with isofluorane, then stimulated with 50 μg poly I:C for 6 hours in a 50 μl inoculum. For viral infections, *Ifnar1*^{SA} and C57BL/6 mice were infected with either PR8 (50-2,000 $TCID_{50}$) or X31 (8,000 $TCID_{50}$) intranasally in a 30-50 μl inoculum. *Mx1*$^{+/+}$ *Ifnar1*^{SA} and *Mx1*$^{+/+}$ were infected intranasally with 2,500-25,000 $TCID_{50}$ of hvPR8-NS1(1-126) in 50 μl. *Ifnar1*^{SA}*MxA*$^{tg/tg}$ mice were infected at the University of Freiburg using 2,500 PFU of hvPR8-NS1(1-126) in a 40 μl volume. *Mx1*$^{+/+}$ *Ifnar1*^{SA} and *Mx1*$^{+/+}$ were infected intranasally with $4x10^4$ PFU Udorn virus (Klinkhammer et al., 2018).

Depletion and blockade by antibodies

IFNAR1 blocking antibody was delivered *in vivo* (200 μl of 2 mg/ml intraperitoneally) to block IFNAR1 signaling, as described in the figure legends. pDC depletion of C57BL/6 and *Ifnar1*^{SA} mice was achieved by intraperitoneal injection of mice with 200 μl of anti-PDCA1 antibody at 2 mg/ml.

Differentiation of bone marrow derived cells and primary mouse tracheal epithelial cell culture (mTEC)

Bone marrow derived macrophages (BMDMs) were generated using L929-conditioned media containing M-CSF for 7 days. Cell populations confirmed by CD11b and CD11c expression. For BMDMs cell stimulations, $2x10^5$ BMDMs were plated on flat bottomed 96 well plates, allowed to rest overnight, and stimulated with varying concentrations of IFNα_4. Isolation and culture of primary mTEC were performed as previously described (You et al., 2002). Briefly, cells isolated by enzymatic treatment were seeded onto 0.4 μm transwells (Greiner) coated with a collagen solution. At confluence, media was removed from the upper chamber to establish an air-liquid interface (ALI). Fully differentiated, 10-14 days-old post ALI cultures were routinely used for experiments.

CD45 isolation from lung tissue

Single cell suspensions acquired as described in the flow cytometry materials and methods section. CD45+/− separation was achieved by MACS magnetic separation columns according to manufacturer specifications. Briefly, pelleted cells were resuspended in MACS buffer + 10 μl CD45 microbeads per 10^7 cells, and incubated for 15 min at 4°C. Labeled cells were added to equilibrated magnetic separation columns (LS column, Miltenyi), and washed three times in the presence of a strong magnet. Both positive and negative fractions were collected, pelleted by centrifugation, and resuspended in the appropriate amount of RLT buffer according to manufacturer instructions (QIAGEN). RNA isolated, and cDNA synthesized as described above.

RNaseq

RNA extracted from MACS-separated lung $CD45^-$ cells was normalized to 1 ng and cDNA synthesis was performed using the Ovation RNA-Seq System V2 with 8 PCR cycles. Libraries were constructed from cDNA using the Ovation Ultralow System V2 with 100 ng cDNA input and 8 PCR cycles. Sequencing was performed on the HiSeq 4000 system (Illumina) with Single End 75 bp reads.

Read quality trimming and adaptor removal was carried out using Trimmomatic (version 0.36). Reads were aligned to the mouse genome (Ensembl GRCm38 release 89) using STAR (version 2.5.2a) and gene level counts were obtained using the RSEM package (version 1.2.31). For RSEM, all parameters were run as default except "–forward-prob" that was set to 0.5. Differential expression analysis was carried out with DESeq2 package (version 1.20.0) within R version 3.5.1. Genes were considered to be differential expressed with padj $\leq$ 0.05.

Gene Set Enrichment analysis (GSEA, version 2.2.3) was performed for each pairwise comparison using gene lists ranked using the Wald statistic. Geneset pre-ranked analysis was carried with respect of genesets C2 canonical pathways v5.2 and C5 biological processes v5.2. All parameters were kept as default except for enrichment statistic that was changed to classic and the max size which was changed to 500,000. Gene signatures were considered significant if FDR q-value $\leq$ 0.05.

Flow cytometry analysis

Harvested lung tissue from infected and naive animals were processed into single cell suspensions by digestion for 30 min in DNaseI and Liberase at 37°C. Lungs were homogenized in C tubes (Miltenyi) using GentleMax dissociator and passed through a 100 μm filter. After red blood cell lysis, cells were centrifuged and resuspended in 2 mL AB-IMDM (kindly prepared by the Crick Media Preparation STP). Single cell suspensions were incubated with anti-FcγRIII/II for 10 min prior to addition of antibodies for flow cytometry. Cells were incubated with antibodies for 30 min at 4°C, washed and fixed with 4% PFA and subsequently analyzed on a Fortessa cell analyzer (BD Bioscience).

Protein analysis

BAL fluid was recovered from infected mice, centrifuged at 1,300 rpm, 5 min at 4 °C and supernatant collected. Concentrations of IFNα, β and λ were measured by ELISA as per the manufacturer's instructions. Concentrations of CXCL10 and IL-6 were assessed by using 36-Plex Mouse ProcartaPlex Panel as per the manufacturer's instructions and read on a Bio-Plex 200 System (BioRad).

QUANTIFICATION AND STATISTICAL ANALYSIS

All results are expressed as mean ± s.e.m. Statistical significance determined by a p value < 0.05 as determined by either using two-way ANOVA with appropriate multiple corrections test as necessary, unpaired Mann-Whitney U test, or t test. All statistics performed by using GraphPad Prism 7 software. In general, all *in vivo* experiments utilize at least three mice, and each symbol in the graph represents one animal. *In vitro* experiments are performed in triplicates with samples from at least two individual mice. Symbols indicating significance are as follows: p < 0.05 = *; p < 0.01 = **; p < 0.001 = ***; and p < 0.0001 = ****; Sample sizes were dictated to adhere to the UK Home Office 3R principles, while providing appropriate statistical power.

DATA AND CODE AVAILABILITY

The GEO accession number for the RNaseq dataset reported in this paper is GEO: GSE129073.